European Journal of Medicinal Chemistry 44 (2009) 2523–2532

Contents lists available at ScienceDirect

European Journal of Medicinal Chemistry

journal homepage: http://www.elsevier.com/locate/ejmech

Original article

Synthesis, biological evaluation and molecular modeling of oxoisoaporphine and oxoaporphine derivatives as new dual inhibitors of acetylcholinesterase/butyrylcholinesterase

Huang Tang [a,b], Yong-Biao Wei [a], Chi Zhang [a], Fang-Xian Ning [a], Wei Qiao [b], Shi-Liang Huang [a], Lin Ma [b], Zhi-Shu Huang [a,*], Lian-Quan Gu [a,b,**]

[a] School of Pharmaceutical Sciences, Sun Yat-sen University, Guangzhou 510006, China
[b] School of Chemistry and Chemical Engineering, Sun Yat-sen University, Guangzhou 510275, China

ARTICLE INFO

Article history:
Received 9 August 2008
Accepted 22 January 2009
Available online 31 January 2009

Keywords:
Oxoaporphine derivatives
Oxoisoaporphine derivatives
Synthesis
Acetylcholinesterase inhibitors
Butyrylcholinesterase inhibitors

ABSTRACT

Aporphine alkaloids, isolated from Chinese medicinal herb, are important natural products. We recently reported that synthetic derivatives of oxoisoaporphine alkaloids exhibited high acetylcholinesterase inhibitory activity and high selectivity for AChE over BuChE (Bioorg. Med. Chem. Lett. 2007, 17, 3765–3768). In this paper, further research results were presented. A series of novel derivatives of oxoaporphine alkaloids (**5a–j**, 4-carboxylic amide-7-oxo-7*H*-dibenzo[*de*,*g*]quinoline, Ar-CONH$(CH_2)_n$NR) and their quaternary methiodide salts (**6a–h**, Ar-CONH$(CH_2)_n N^+(CH_3)RI^-$) were designed and synthesized as acetylcholinesterase (AChE) and/or butyrylcholinesterase (BuChE) inhibitors. The AChE inhibition potency of synthetic oxoaporphine derivatives was decreased about 2–3 orders of magnitude as compared with that of oxoisoaporphine derivatives. Non-competitive binding mode was found for both kinds of derivatives. Molecular docking simulations on the oxoisoaporphine derivatives **7** series and oxoaporphine derivatives **6** series with AChE from *Torpedo californica* have demonstrated that the ligands bound to the dual-site of the enzyme.

1. Introduction

Alzheimer's disease (AD) is a progressive neurodegenerative disorder which is one of the most common causes of mental deterioration in elderly people. Current treatment approaches in this disease continue being primarily symptomatic, with the major therapeutic strategy based on the cholinergic hypothesis [1,2] and specifically on acetylcholinesterase inhibition [3–5].

Acetylcholinesterase (EC 3.1.1.7, AChE) is a cholinesterase. Terminating the impulse transmission at cholinergic synapses rapid hydrolysis by AChE into acetylcholine (ACh) is the vital function of AChE. Recent study showed that AChE could also play a key role in accelerating senile amyloid β-peptide (Aβ) plaques deposition [6]. It was likely that AChE interacted with Aβ and promoted amyloid fibril formation through a pool of amino acids located in the proximity of peripheral anionic site (PAS) [7]. Furthermore it has been reported that this activity was blocked by the peripheral site inhibitor propidium (**A**, Fig. 1), but not by the active site inhibitor edrophonium (**B**, Fig. 1) [8]. It implied that AChE inhibitors that were recognized at the PAS or interact with both the catalytic site and PAS might exert a dual pharmacological effect [1], which combined the enhancement of the cholinergic neurotransmission and the reduction in the pro-aggregating action of AChE, thus opening the way to a new promising therapeutic approach to Alzheimer's disease (AD). Following this rationale, a number of studies had been performed, such as tacrine–melatonin hybrids (**C**, Fig. 1). It was reported that their IC_{50} values range from sub-nanomolar to picomolar [9]. The primary requirement for this high inhibitory activity was for an aromatic pharmacophore capable of binding to PAS by means of π–π interactions. The another pharmacophore that linked by alkylene is also required, which molecular modeling studies had suggested that this pharmacophore was directed toward anionic subsite of AChE [10,11].

Based on our preceding studies [12], which the synthetic oxoisoaporphine derivatives (**D**, Fig. 1) exhibited high AChE inhibitory activity with IC_{50} values in the nanomolar range and

* Corresponding author. Tel./fax: +86 20 39943056.
** Corresponding author. School of Pharmaceutical Sciences, Sun Yat-sen University, Guangzhou 510006, China.
E-mail addresses: ceshzs@mail.sysu.edu.cn (Z.-S. Huang), cesglq@mail.sysu.edu.cn (L.-Q. Gu).

0223-5234/$ – see front matter © 2009 Elsevier Masson SAS. All rights reserved.
doi:10.1016/j.ejmech.2009.01.021

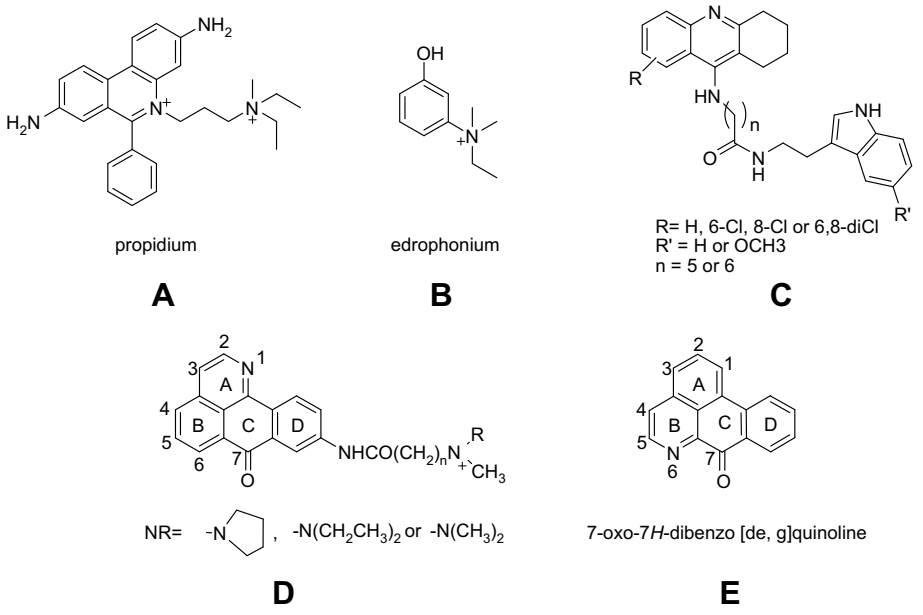

Fig. 1. Chemical structures of some inhibitors of AChE.

high selectivity for AChE over BuChE (45- to 1980-fold). In this paper, according to the SAR results obtained from previous work, we newly synthesized oxoisoaporphine derivatives **7a**, 9-(3-piperidinopropionamido)-1-azabenzanthrone methiodide salt (Fig. 2), which prospectively showed the most powerful inhibitory potency toward AChE with IC_{50} value in sub-nanomolar level. In addition, considering oxoaporphine alkaloids, a isomer of oxoisoaporphine alkaloids, had been isolated from plant species of many genera [13], and a remarkable range of biological activity was found for these alkaloids, such as cytotoxicity to many human cancer cells [14,15], acting against Gram-positive bacteria, yeasts, and filamentous fungi [16,17]. We believed that oxoaporphine derivatives could also act as dual inhibitors of AChE by modified structure. Oxoaporphine alkaloids possess a 7-oxo-7*H*-dibenzo[*de*,*g*]quinoline moiety in their structures (**E**, Fig. 1). The only difference between oxoaporphine and oxoisoaporphine alkaloids is the position of nitrogen atom in the pharmacophore. In this paper, a series of oxoaporphine derivatives (**5a**–**j** and **6a**–**h** in Fig. 2) with different basic side chains at 4-position of 7-oxo-7*H*-dibenzo[*de*,*g*]quinoline (general formula is Ar-CONH$(CH_2)_n$NR, Ar = 7-oxo-7*H*-dibenzo[*de*,*g*]-quinoline, $n = 2$ or 3) were designed and synthesized, and their anti-AChE and BuChE activities were tested. The docking program by computational modeling was also performed.

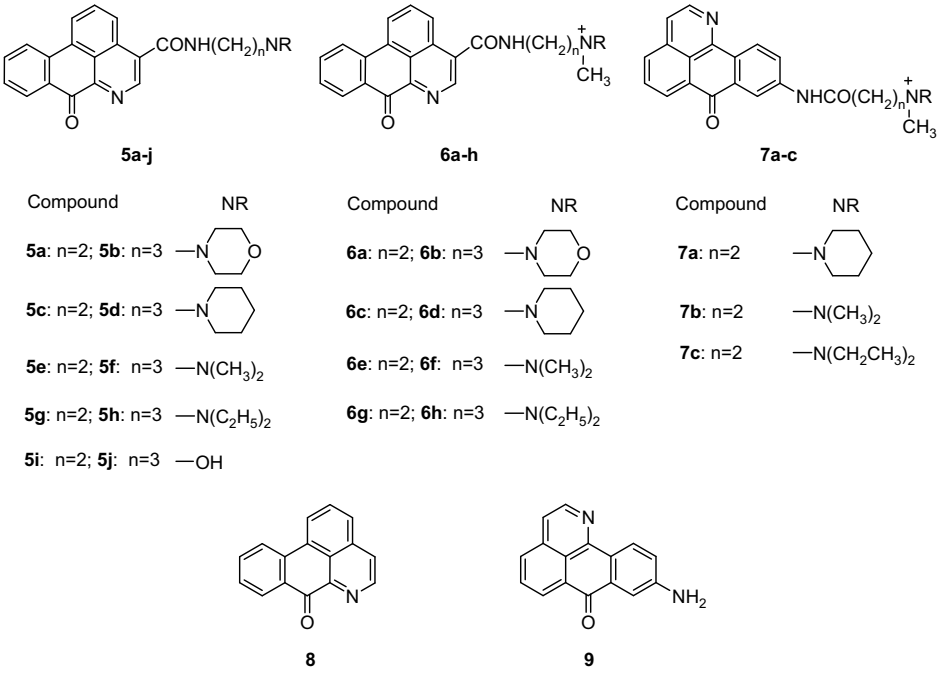

Fig. 2. Structures of oxoaporphine derivatives **5a**–**j** and **6a**–**h**.

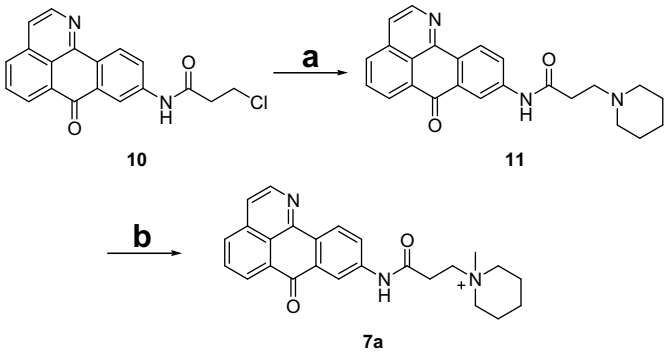

Scheme 1. Synthesis of 9-(3-piperidinopropionamido)-1-azabenzanthrone methiodide salt. Reagents and conditions: (a) Piperidine /EtOH/NaI/reflux; (b) $CH_3I/CHCl_3$/rt/24 h.

2. Results and discussion

2.1. Chemistry

Preparation of oxoaporphine derivatives **7b** and **7c** (Fig. 2) investigated in this study had been previously described [12]. The newly synthetic 9-(3-piperidinopropionamido)-1-azabenzanthrone methiodide salt (**7a**, Fig. 2) was obtained, following similar procedures, as shown in Scheme 1.

Synthesis of 4-carboxylic amide-7-oxo-7*H*-dibenzo[*de*,*g*]quinoline **5a**–**j** and **6a**–**h** was accomplished as described in Scheme 2. Preparation of dimethyl 7-oxo-7*H*-dibenzo[*de*,*g*]quinoline-4,5-dicarboxylate **2** was carried out by a reported method [18]. Hydrolysis of compound **2** using potassium hydroxide gave 4,5-dicarboxyl-7-oxo-7*H*-dibenzo[*de*,*g*]quinoline **3** in 92% yield. 4-Carboxyl-7-oxo-7*H*-dibenzo[*de*,*g*]quinoline **4** was obtained in 73% yield by decarboxylation of **3** in diphenyl ether at 190 °C for 1.5 h. Amidification of **4** when treated with appropriate amines was failed when we used several classical coupling agents such as ethyl chloroformate, DCC–DMAP [19]. However, using PyBOP [20,21] in *N*,*N*-dimethyl acetamide (DMA), which generally worked with hindered carboxylic acids, the desired amides **5a**–**j** were obtained in good yields (51–68%). The corresponding quaternary methiodide salts **6a**–**h** were obtained by treatment with CH_3I in $CHCl_3$. Finally, in order to know the inhibitory potency of chromophore, 7-oxo-7*H*-dibenzo[*de*,*g*]quinoline (**8**, Fig. 2) was also synthesized.

The position of carboxyl group in compound **4** was determined by Nuclear Magnetic Resonance technology. ^{1}H NMR spectra of compounds **4** and **8** are shown in Fig. 3 with the given structures. ^{1}H NMR spectrum revealed that H-4 (δ 8.27 ppm) and H-5 (δ 9.00 ppm) proton signals in compound **8** appeared as doublets peak sharing a unique coupling constant of 5.3 Hz, and H-3 proton signal appeared at δ 8.19 ppm as a doublet peak exhibiting a coupling constant of 8.0 Hz. Reviewing ^{1}H NMR spectrum of compound **4**, since a strong electronic effect of the carboxyl group at C-4 on H-3 and H-5 existed, a clear downfield chemical shift at δ 8.87 ppm for H-3 and δ 9.36 ppm for H-5 was observed, and with the disappearance of splitting signal on H-5.

2.2. Biological activity studies

Inhibitory activities toward AChE and BuChE *in vitro* of synthetic compounds were determined according to the modified Ellman method [22] using commercially available galanthamine as the reference standard. AChE [23] from *electric eel* and BuChE from *equine serum* were purchased from Sigma Corporation.

The IC_{50} values for AChE and BuChE inhibition are summarized in Table 1. All the synthetic oxoaporphine derivatives with quaternary nitrogen demonstrated much higher inhibitory potent against AChE than the lead compound **8** and inhibitory activity with IC_{50} values ranging from micromolar to sub-micromolar. This result indicated that introduction of the amino group side chains could increase the inhibitory capacity. Structural resembling of quaternary functionality between the synthesized cationic compounds and ACh would be responsible for competition of the binding site of AChE. Compounds **5i**–**j** which possessed hydroxyl group at the end of side chain exhibited much weaker anti-AChE activity even weaker than lead compound **8**. These phenomena implied that pK_a values of the side chain might play a significant role in influencing activity. The attachment of terminal group with low pK_a values to the side chain could limit the access of compounds to the anionic subsite of AChE.

According to the screening data, the structure of terminal groups -NR of side chain has also effects on their inhibitory

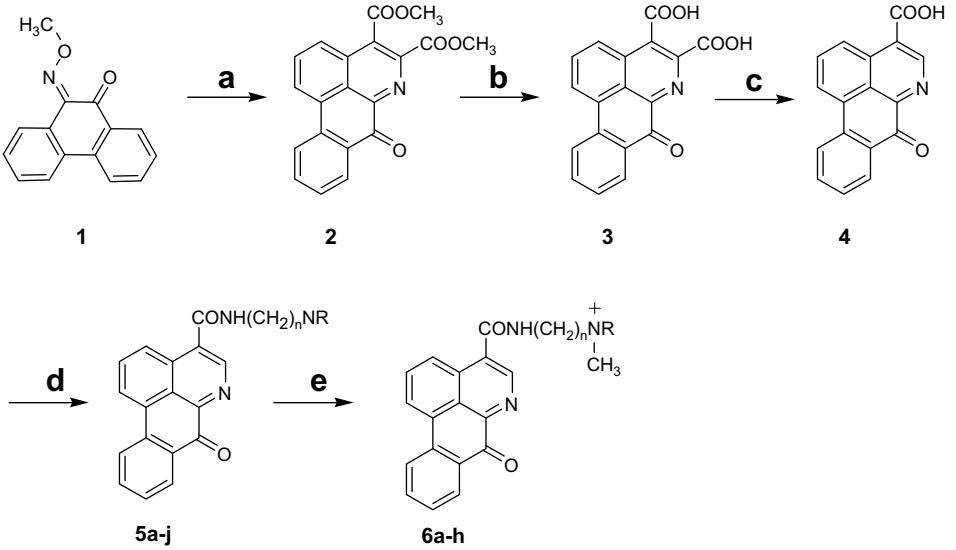

Scheme 2. Synthesis of oxoaporphine derivatives. Reagents and conditions: (a) DMAD/toluene/reflux /8 days; (b) $KOH/CH_3OH/H_2O$ (65 °C); (c) diphenyl ether (190 °C); (d) $NH_2(CH_2)_nNR/PyBOP/DMF$ (65 °C); (e) $CH_3I/CHCl_3$/rt/24 h.

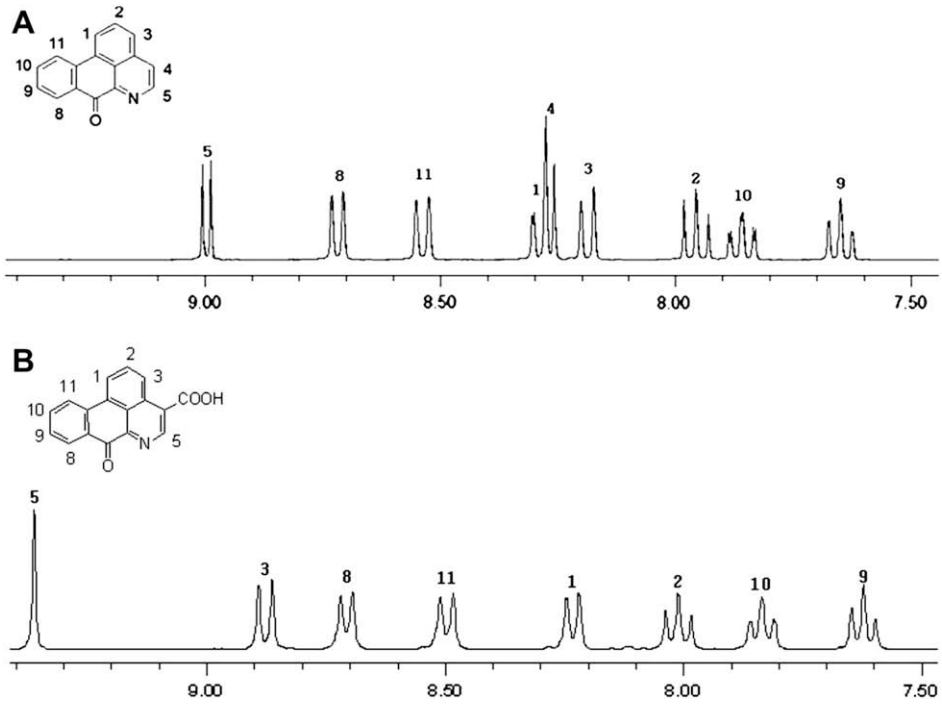

Fig. 3. (A) ^{1}H NMR spectrum (300 MHz) of **8** in DMSO; (B) ^{1}H NMR spectrum (300 MHz) of **4** in $CDCl_3$.

activities (Table 1 and Fig. 4). The results were the same with the reported oxoisoaporphine derivatives [12]. High inhibitory potency was found to be associated with piperidine at the end of side chain (**6c–d**). Dimethylamine derivatives showed less potent (**6e–f**), which caused approximately 9- to 30-fold decrease compared with piperidine derivatives in activity. The congeners with bulkier substituent (compounds **6c–d** and **6g–h**) led to a huge increase in activity than that bearing small ones (compounds **6e–f**), indicating the semirigid side chain could be in favor of accessing terminal groups to the enzyme-binding site.

Both kinds of leader compounds **8** and **9** exhibited similar inhibitory potency toward AChE in same magnitude order. However, their inhibitory potency toward BuChE was different. Compound **8** was more potent of inhibitory activity against BuChE than that of AChE. On the contrary, compound **9** exhibited insignificant inhibitory potency toward BuChE. The nature of AChE

Table 1
In vitro inhibition and selectivity of compounds **8**, **9**, **5i–j**, **6a–h**, **7a–c** and galanthamine on AChE and BuChE.

Compd.	NR	*n*	$IC_{50}$for AChE[a] (μM)	IC_{50} for BuChE[b] (μM)	Selectivity for AChE/BuChE[c]
8	–	–	10.57 ± 0.35	4.01 ± 0.16	0.4
9[d]	–	–	26.9 ± 1.43	>100	>4
6a		2	1.24 ± 0.35	11.69 ± 0.37	9
6b		3	1.05 ± 0.15	4.75 ± 0.22	4
6c		2	0.35 ± 0.09	6.76 ± 0.32	16
6d		3	0.11 ± 0.07	6.24 ± 0.25	57
7a		2	$4.8 \times 10^{-4} \pm 0.8 \times 10^{-4}$	0.60 ± 0.02	1250
6e	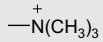	2	3.32 ± 0.29	5.03 ± 0.12	1
6f		3	3.16 ± 0.33	2.71 ± 0.18	1
7b[d]		2	$4.81 \times 10^{-3} \pm 0.4 \times 10^{-3}$	2.82 ± 0.02	590
6g	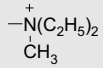	2	1.71 ± 0.26	8.14 ± 0.16	5
6h		3	0.65 ± 0.16	9.72 ± 0.29	15
7c[d]		2	$2.62 \times 10^{-3} \pm 0.2 \times 10^{-3}$	5.19 ± 0.08	1980
5i	–OH	2	17.99 ± 0.87	68.73 ± 1.04	4
5j		3	12.16 ± 0.83	53.25 ± 1.07	4
G[e]			0.55 ± 0.09	14.40 ± 0.12	26

[a] IC_{50}: 50% inhibitory concentration (means ± SEM of three experiments) of AChE.
[b] IC_{50}: 50% inhibitory concentration (means ± SEM of three experiments) of BuChE.
[c] Selectivity for AChE = IC_{50} (BuChE)/IC_{50} (AChE).
[d] Value from Ref. [10].
[e] Galanthamine.

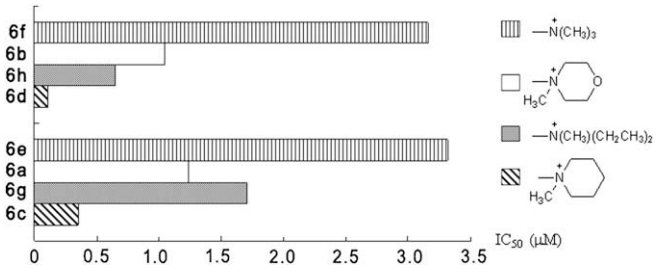

Fig. 4. Effects of structure of terminal groups on AChE.

inhibition caused by these two compounds was investigated by the graphical analysis of steady-state inhibition data (Fig. 5A and C), and the *K*i values are reported in Table 2. Reciprocal plots (Lineweaver–Burk plots) describing **8** and **9** inhibition showed both increasing slopes and increasing intercepts with higher inhibitor concentration compared to **7a** and **6d**. This pattern indicated the mixed inhibition which was similar to that of tacrine. Different inhibitory potencies toward BuChE might be understood that compound **8** was more favorable of binding to active site of both enzymes as compared to compound **9**, since BuChE possessed similar active site compared with that of AChE and was the lack of the PAS moiety [24].

Interestingly, introducing side chains into both kinds of chromophore not only increased their inhibitory selectivity for AChE/BuChE but also changed their type of inhibition. The graphical analysis of steady-state inhibition data for representative compounds **7a** and **6d** is shown in Fig. 5B and D, respectively, and the estimates of inhibition constants K_i are also reported in Table 2. In the reciprocal plots of Fig. 5B and D, lines crossing the *x* axis in the same point revealed that unchanged K_m and decreased V_{max} with increasing inhibitor concentrations. This is a typical trend for non-competitive inhibition which was similar to that of propidium [25].

In addition, compounds **7a** and **7c** showed strongest potent inhibitory activity against AChE and also demonstrated a high selectivity for AChE over BuChE. The results presented in Table 1 suggested that the phenomenological correlation between anti-AChE activity and selectivity for AChE/BuChE. The compounds showed higher inhibitory potential against AChE that would possess higher AChE/BuChE selectivity ratios.

Recently, Inestrosa [7,26] and Bartolini et al. [27] pointed out that AChE could also accelerate Aβ deposition, and that such a noncatalytic action might be mediated by the interaction of Aβ with residues located in the vicinity of the PAS. Thus, BuChE which lacked some key amino acids in its peripheral site was not known to promote the β-amyloid formation [28]. The study [27] on the effect of several AChE reversible inhibitors on the Aβ aggregation induced by recombinant hAChE showed that propidium, which has a non-competitive inhibition type, showed a significant decrease in the Aβ aggregation (by around 82% at 100 μM concentration), which can be attributed to its high affinity for the PAS. In contrast,

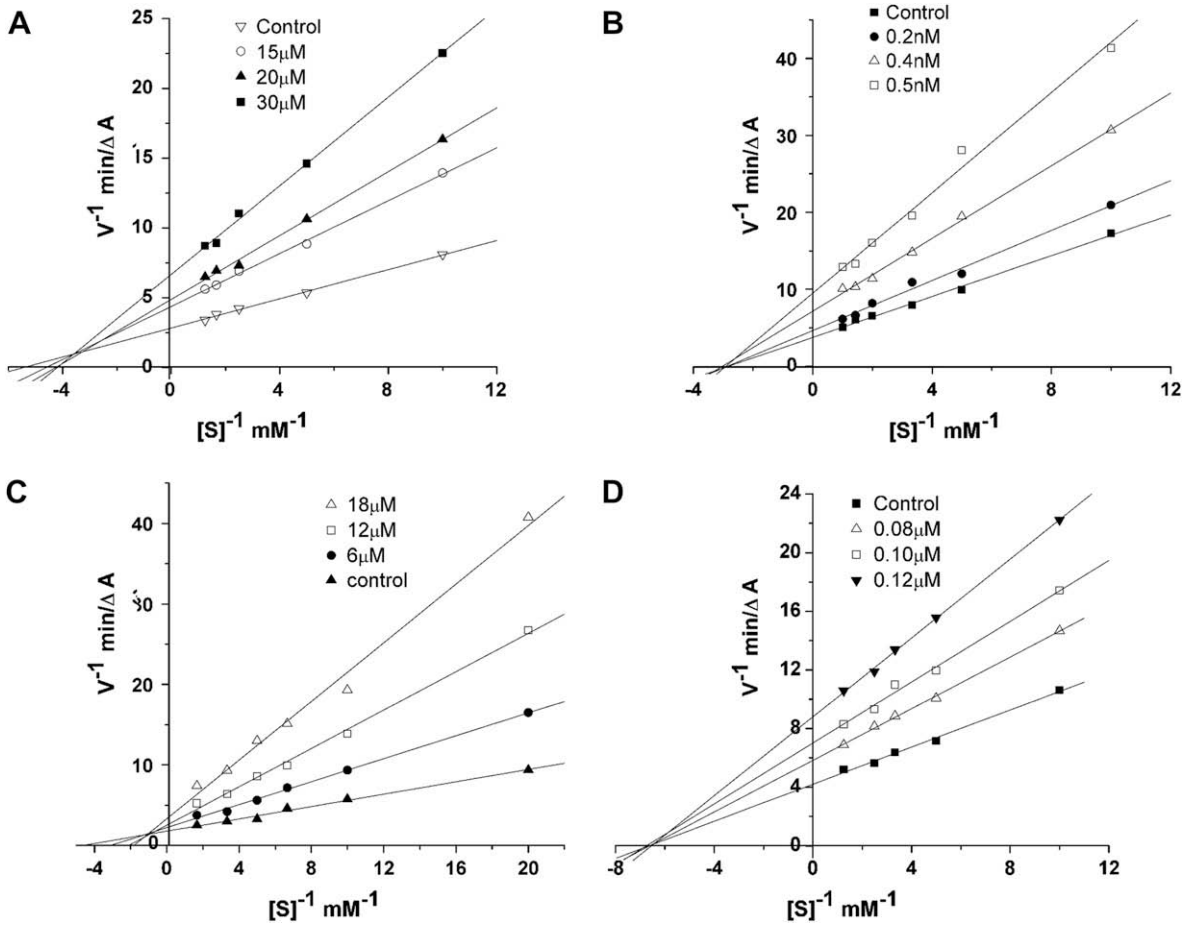

Fig. 5. Steady state inhibition by **8** (A), **7a** (B), **9** (C) and **6d** (D) of AChE hydrolysis of ATCh; (A–D) reciprocal plots of initial velocity and substrate concentration: the plots show mixed-type inhibition for **8** (A) and **9** (C), and non-competitive inhibition for **7a** (B) and **6d** (D).

Table 2
AChE inhibition constants of some selected derivatives.

Compound	$K_i \pm$ SE (μM)	Type of inhibition
8	14.58 ± 1.92	Mixed
7a	0.00031 ± 0.00003	Non-competitive
9	3.86 ± 1.11	Mixed
6d	0.11 ± 0.025	Non-competitive

edrophonium, an active site inhibitor, did not show any effect on the hAChE-induced βA fibrillogenesis. Tacrine, which has a mixed inhibition type, had a small effect (around 7%), which can be attributed to its higher affinity for the active site than for the PAS [27,29]. It could imply that an inhibitor of AChE that strongly interacted with the PAS would show high AChE/BuChE selectivity, and eventually perform inhibitory effect against AChE-induced Aβ aggregation. So, our finding is particularly interesting in the connection to the Alzheimer's disease, because synthetic derivatives with the binding mode similar to that of propidium showed strong inhibitory activity against AChE.

2.3. Molecular modeling studies

In order to further investigate the interaction mode of oxoisoaporphine and oxoaporphine derivatives to AChE, molecular modeling methods including docking and molecular dynamics (MD) simulations were performed. The X-ray crystal structure of bifunctional inhibitor bis(5)-tacrine complexed with *Torpedo californica* AChE [10] was used to build the starting model. In this structure, residue Phe 330 which formed the "bottle neck" of the active site gorge adopts an "open" conformation, allowing larger chemical groups to reach the base of the gorge. All the compounds were flexibly docked into the binding site comprising the central catalytic pocket and peripheral sites.

The position of compounds **7a** and **6d** with respect to the key residues in the binding site is shown in Fig. 6. Compound **7a** (see Fig. 6 left) with the strongest inhibitory potency, could bind with the choline binding site and peripheral anionic site simultaneously. Its coplanar isoquinoline moiety could stack above PAS residue Trp 279, and this interaction maintained during the course of MD simulations. The distance between the centroid of isoquinoline ring and the Trp 279 aromatic ring varied from 4.4 to 5.0 Å, which indicated a typical π–π interaction. The conformation of the side chain made good fit with the shape of the gorge, and its amide moiety could form hydrogen bonds with Tyr 121 and Asp 72. The protonated terminal piperidine group placed between Trp 84 and Phe 330, making cation–π interactions with aromatic rings in both residues in a "sandwich" form. This structure was also found to be stable in MD simulations, and acted as one of the major interactions between ligand and AChE. By aligning the conformation of **7a** to the original ligand of the X-ray structure bis(5)-tacrine (Fig. 7), it could be easily found out that both molecules could arrange themselves in order to make best of their possibility to establish interactions with choline binding site and PAS residues. The number of atom between piperidine N and isoquinoline in **7a** (7 atoms) was equal to the length of tether between two tacrine moieties in bis(5)-tacrine. It indicated that the length between two functional groups in oxoisoaporphine derivatives contributed greatly to its activity.

Oxoaporphine derivative, such as **6d** (see Fig. 6 right), shared a similar interaction mode with **7a** as a result from modeling studies. Its aromatic moiety could also form π–π stack with Trp 279, and piperidine was firmly bound to the catalytic site of AChE, it being stacked against the aromatic rings of Trp 84 and Phe 330. However, the orientation of the scaffold in **6d** had changed. In order to allow the 4-positioned side chain probe deeper into the gorge, the isoquinoline ring can no longer reach Trp 279, and thus made the interaction weaker. It was the key reason for explaining that oxoisoaporphine derivatives showed higher inhibitory potency than oxoaporphine derivatives. Furthermore, geometric clashes were detected between the isoquinoline moiety in **6d** and the "bottle neck" residues (Phe 330 and Tyr 121), preventing the scaffold from moving so deep as oxoisoaporphine derivatives.

The interaction energy between modeled compounds and AChE was further evaluated by LigScore2 [31] and PLP2 [32] scoring functions (Table 3). The calculated interaction score was found to correlate well with experimental binding free energies (LigScore2 $r = -0.855$, PLP2 $r = -0.831$). It indicated that these scoring functions may serve as a quick method to distinguish the potency of newly designed compounds.

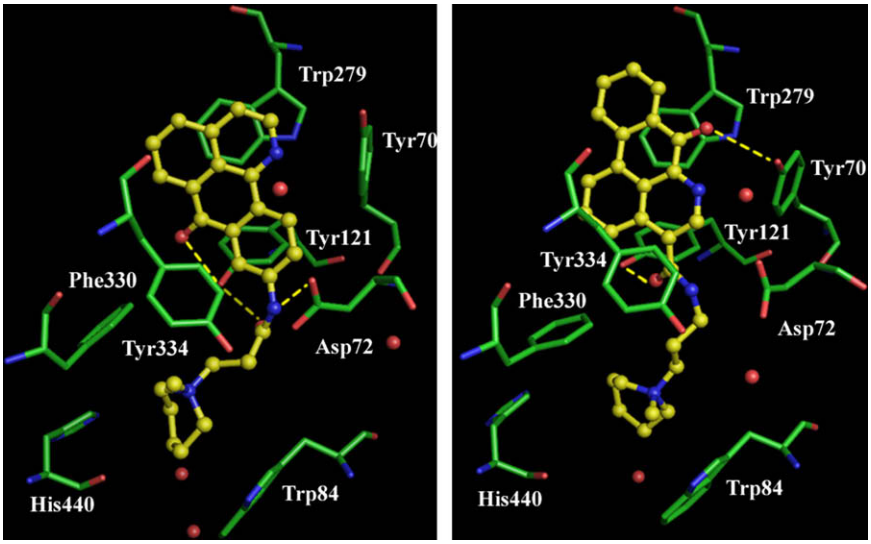

Fig. 6. Representations of compounds **7a** (left) and **6d** (right) interacting with residues in the binding site of *Tc*AChE. The compounds are rendered in yellow ball-and-stick models, and the residues are rendered in green colored sticks. Hydrogen bonds are shown in yellow dotted lines. Pictures are created with PyMOL [30]. (For interpretation of the references to colour in this figure legend, the reader is referred to the web version of this article.)

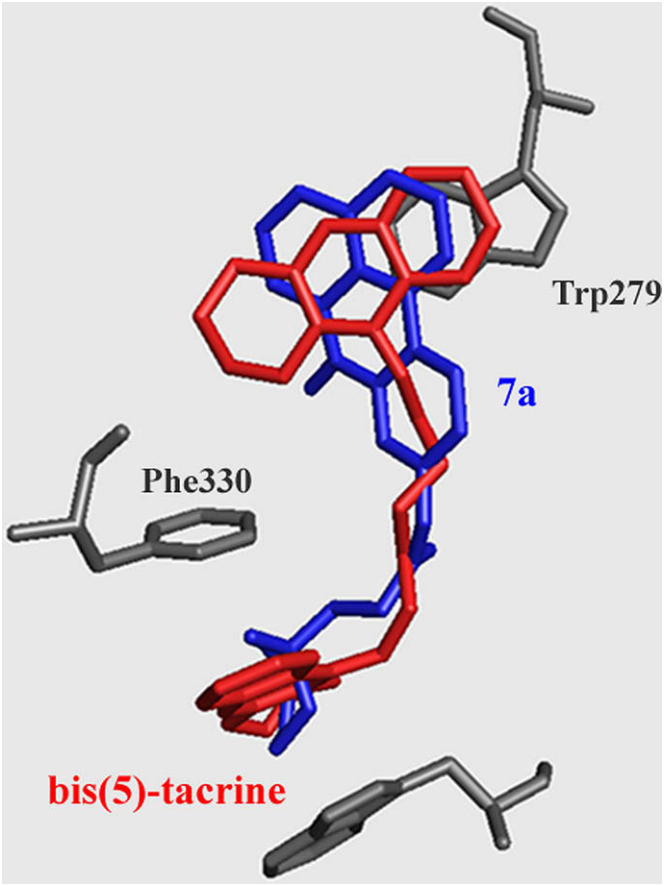

Fig. 7. Superposition of modeled structure of compound **7a** (colored in blue) with X-ray crystal structure of TcAChE binding with bis(5)-tacrine (colored in red, PDB entry: 2CMF). (For interpretation of the references to colour in this figure legend, the reader is referred to the web version of this article.)

In conclusions, all synthetic oxoisoaporphine and oxoaporphine derivatives showed inhibitory potency toward AChE. Non-competitive binding mode was found for both kinds of derivatives. However, their inhibitory activity toward AChE and their selectivity for AChE/BuChE were much different. Molecular modeling indicated that the capacity of interacting with peripheral anionic site of acetylcholinesterase, especially with Trp 279 of PAS, would be responsible for the results. That was to say, a inhibitor that to be strongly interacting with the PAS would not only exhibit strong inhibitory potency toward AChE but also show high AChE/BuChE selectivity. We hope that this work could be beneficent for the development potential of AChE inhibitors with higher inhibitory activity and good selectivity for AChE over BuChE in the future.

Table 3
The predicted interaction energy evaluated by LigScore2 and PLP2 scoring functions and the observed binding free energy.

Compound	LigScore2[a]	PLP2	Experimental ΔG[b] (in kcal/mol)
5i	6.08	110.71	−6.45
5j	5.90	110.50	−6.68
6a	6.23	115.12	−8.02
6b	6.16	113.16	−8.12
6c	6.07	112.76	−8.77
6d	6.44	114.82	−9.45
6e	6.30	118.77	−7.44
6f	5.75	107.86	−7.47
6g	6.44	111.32	−7.83
6h	6.69	115.20	−8.40
7a	6.99	121.83	−12.66
7b	6.82	125.35	−11.30
7c	7.08	122.82	−11.66

[a] Dreiding force field was employed for calculation.
[b] $\Delta G = RT \ln(IC_{50})$, where $T = 298$ K.

3. Experimental section

3.1. Chemistry

UV/visible absorbance spectra were measured on a Shimadzu UV-2450 spectrophotometer. ESI-MS spectra were obtained using an LCMS-2010A Mass Spectrometer. ^{1}H NMR spectra were performed on a Varian Mercury-Plus 300 NMR Spectrometer with tetramethylsilane (TMS) as an internal standard. Elemental analysis was carried out on an Elementar Vario EL CHNS Elemental Analyzer.

3.1.1. *Dimethyl 7-oxo-7*H*-dibenzo[*de,*g]quinoline-4,5-dicarboxylate (**2**)*

A solution of (**1**) (23.7 g, 0.1 mol) and dimethyl acetylenedicarboxylate (DMAD) (31.2 g, 0.22 mol) in toluene (400 mL) was refluxed for 8 days and then set aside overnight during which time yellow crystals separated. The crystalline solid was filtered off and was further purified by recrystallization from chloroform to give **2** (8.8 g, 25%), m.p. 271–273 °C (lit. [18], 268–272 °C). ^{1}H NMR ($CDCl_3$): δ_H 4.09 (*s*, 3H), 4.14 (*s*, 3H), 7.60 (*t*, 1H, $J = 7.3$ Hz), 7.78 (*t*, 1H, $J = 7.3$ Hz), 7.93–8.04 (*m*, 2H), 8.25 (*d*, 1H, $J = 8.1$ Hz), 8.47–8.54 (*m*, 2H). ESI-MS *m*/*z*: 348 $[M + H]^+$.

3.1.2. *4,5-Dicarboxyl-7-oxo-7*H*-dibenzo[*de,*g]quinoline (**3**)*

To a stirred suspension of **2** (3.5 g, 0.01 mol) in methanol (40 mL) was added a solution of KOH (3 g, 0.05 mol) in water (100 mL). The mixture was heated at reflux for 24 h and left to stand overnight. The methanol was removed in vacuo and to the aqueous solution was added 1 N HCl until pH = 1–2. The yellow solid was filtered off and was purified by crystallization from nitrobenzene to afford **3** (2.9 g, 92%). Amorphous powder. ^{1}H NMR (DMSO): δ_H 7.69 (*t*, 1H, $J = 7.5$ Hz), 7.91 (*t*, 1H, $J = 7.5$ Hz), 8.09–8.18 (*m*, 2H), 8.31 (*d*, 1H, $J = 7.7$ Hz), 8.61 (*d*, 1H, $J = 8.0$ Hz), 8.90 (*d*, 1H, $J = 7.0$ Hz). ESI-MS *m*/*z*: 318 $[M - H]^-$.

3.1.3. *4-Carboxyl-7-oxo-7*H*-dibenzo[*de,*g]quinoline (**4**)*

Compound **3** (3.2 g, 0.01 mol) in diphenyl ether (20 mL) was heated at 190 °C for 1.5 h. The mixture was then cooled to room temperature. The brown-yellow solid was filtered off and washed with ether. The compound **4** (2.0 g, 73%) was purified by crystallization from nitrobenzene. Amorphous powder. ^{1}H NMR (DMSO): δ_H 7.62 (*t*, 1H, $J = 7.4$ Hz), 7.84 (*t*, 1H, $J = 7.4$ Hz), 8.01 (*t*, 1H, $J = 8.4$ Hz), 8.23 (*d*, 1H, $J = 7.8$ Hz), 8.50 (*d*, 1H, $J = 8.0$ Hz), 8.71 (*d*, 1H, $J = 7.4$ Hz), 8.87 (*d*, 1H, $J = 8.0$ Hz), 9.36 (*s*, 1H). ESI-MS *m*/*z*: 274 $[M - H]^-$.

3.1.4. *7-Oxo-7*H*-dibenzo[*de,*g]quinoline-4-carboxyl (2-morpholinoethyl)amide (**5a**)*

General Acylation Procedure: PyBOP (2.0 g, 3.8 mmol) in DMA (3 mL) was added over 30 min period to a solution of compound **4** (0.55 g, 2 mmol) and 2-(morpholine)ethylamine (180 μL) in DMA (4 mL) at 65 °C. The mixture was stirred at 65 °C for 1 h and concentrated under vacuum. The residue was taken up with dichloromethane and the solution washed with a solution of sodium carbonate, dried (Na_2SO_4), and concentrated under vacuum. Column chromatography of the residue, eluting with a 5% methanol in dichloromethane, gave compound **5a** (0.48 g, 62%). ^{1}H NMR ($CDCl_3$): δ_H 2.17 (*m*, 2H), 2.62 (*m*, 4H), 2.77 (*t*, 2H, $J = 5.7$ Hz),

3.75 (*m*, 4H), 7.55 (*t*, 1H, *J* = 7.8 Hz), 7.68 (*t*, 1H, *J* = 7.8 Hz), 7.73 (*t*, 1H, *J* = 7.3 Hz), 8.10 (*d*, 1H, *J* = 8.0 Hz), 8.17 (*d*, 1H, *J* = 7.3 Hz), 8.37–8.39 (*m*, 2H), 8.98 (*s*, 1H). ESI-MS *m*/*z*: 388 $[M+H]^+$. Anal. Calcd for $C_{23}H_{21}N_3O_3 \cdot 2H_2O$: C, 65.24; H, 5.95; N, 9.92. Found: C, 65.05; H, 6.09; N, 9.78.

As described for **5a**, using the appropriate amines, the following compounds were obtained.

3.1.5. 7-Oxo-7H-dibenzo[de,g]quinoline-4-carboxyl (3-morpholinopropyl)amide (**5b**)

Compound **4** was treated with 3-(morpholine)propylamine according to general acylation procedure to give **5b** (58%) as yellow solid. ^{1}H NMR ($CDCl_3$): δ_H 1.94 (*m*, 2H), 2.49 (*t*, 4H, *J* = 4.6 Hz), 2.63 (*t*, 2H, *J* = 6.3 Hz), 3.50 (*t*, 4H, *J* = 4.6 Hz), 3.74 (*q*, 2H, *J* = 5.8 Hz), 7.57 (*t*, 1H, *J* = 8.0 Hz), 7.72–7.81 (*m*, 2H), 8.17 (*d*, 1H, *J* = 8.0 Hz), 8.30 (*d*, 1H, *J* = 7.3 Hz), 8.38 (*d*, 1H, *J* = 7.3 Hz), 8.44 (*dd*, 1H, J_1 = 8.0 Hz, J_2 = 1.3 Hz), 9.01 (*s*, 1H), 8.33 (*t*, 1H, *J* = 4.5 Hz); ESI-MS *m*/*z*: 402 $[M+H]^+$. Anal. Calcd for $C_{24}H_{23}N_3O_3 \cdot 3H_2O$: C, 63.28; H, 6.42; N, 9.22. Found: C, 63.06; H, 6.47; N, 8.96.

3.1.6. 7-Oxo-7H-dibenzo[de,g]quinoline-4-carboxyl (2-piperidinoethyl)amide (**5c**)

Compound **4** was treated with 2-(piperidino)ethylamine according to general acylation procedure to give **5c** (51%) as yellow solid. ^{1}H NMR ($CDCl_3$): δ_H 1.48–1.51 (*m*, 2H), 1.58–1.65 (*m*, 4H), 2.52 (*m*, 4H), 2.69 (*t*, 2H, *J* = 6.0 Hz), 3.71 (*q*, 2H, *J* = 5.6 Hz), 7.56 (*t*, 1H, *J* = 7.6 Hz), 7.74 (*t*, 1H, *J* = 8.0 Hz), 7.79 (*t*, 1H, *J* = 7.5 Hz), 8.18 (*d*, 1H, *J* = 8.0 Hz), 8.31 (*d*, 1H, *J* = 7.4 Hz), 8.43–8.49 (*m*, 2H), 9.06 (*s*, 1H); ESI-MS *m*/*z*: 386 $[M+H]^+$. Anal. Calcd for $C_{24}H_{23}N_3O_2$: C, 74.78; H, 6.01; N, 10.90. Found: C, 74.64; H, 5.78; N, 10.74.

3.1.7. 7-Oxo-7H-dibenzo[de,g]quinoline-4-carboxyl (3-piperidinopropyl)amide (**5d**)

Compound **4** was treated with 3-(piperidino)propylamine according to general acylation procedure to give **5d** (55%) as yellow/brown solid. ^{1}H NMR ($CDCl_3$): δ_H 1.23–1.27 (*m*, 2H), 1.30–1.33 (*m*, 4H), 1.88–1.96 (*m*, 2H), 2.46 (*m*, 4H), 2.63 (*t*, 2H, *J* = 6.0 Hz), 3.72 (*q*, 2H, *J* = 6.9 Hz), 7.57 (*t*, 1H, *J* = 7.9 Hz), 7.75 (*t*, 1H, *J* = 8.5 Hz), 7.82 (*t*, 1H, *J* = 7.5 Hz), 8.21 (*d*, 1H, *J* = 8.0 Hz), 8.35 (*d*, 1H, *J* = 7.4 Hz), 8.45–8.48 (*m*, 2H), 9.02 (*t*, 1H, *J* = 4.6 Hz), 9.08 (*s*, 1H); ESI-MS *m*/*z*: 400 $[M+H]^+$. Anal. Calcd for $C_{25}H_{25}N_3O_2 \cdot H_2O$: C, 71.92; H, 6.52; N, 10.06. Found: C, 71.67; H, 6.73; N, 9.94.

3.1.8. 7-Oxo-7H-dibenzo[de,g]quinoline-4-carboxyl (2-(dimethylamino)ethyl)amide (**5e**)

Compound **4** was treated with 2-(dimethylamino)ethylamine according to general acylation procedure to give **5e** (58%) as yellow solid. ^{1}H NMR (DMSO): δ_H 2.85 (*s*, 9H), 3.31 (*t*, 2H, *J* = 6.1 Hz), 3.73 (*t*, 2H, *J* = 6.1 Hz), 7.68 (*t*, 1H, *J* = 7.5 Hz), 7.89 (*t*, 1H, *J* = 7.1 Hz), 8.04 (*t*, 1H, *J* = 8.3 Hz), 8.30 (*d*, 1H, *J* = 7.7 Hz), 8.43 (*d*, 1H, *J* = 8.4 Hz), 8.59 (*d*, 1H, *J* = 8.1 Hz), 8.80 (*d*, 1H, *J* = 7.3 Hz), 9.14 (*s*, 1H). ESI-MS *m*/*z*: 346 $[M+H]^+$. Anal. Calcd for $C_{21}H_{19}N_3O_2 \cdot H_2O$: C, 69.41; H, 5.82; N, 11.56. Found: C, 69.47; H, 6.01; N, 11.32.

3.1.9. 7-Oxo-7H-dibenzo[de,g]quinoline-4-carboxyl (3-(dimethylamino) propyl)amide (**5f**)

Compound **4** was treated with 3-(dimethylamino)propylamine according to general acylation procedure to give **5f** (52%) as yellow solid. ^{1}H NMR ($CDCl_3$): δ_H 1.81 (*m*, 2H), 2.34 (*s*, 6H), 2.58 (*t*, 2H, *J* = 7.4 Hz), 3.41 (*t*, 2H, *J* = 6.8 Hz), 7.63 (*t*, 1H, *J* = 7.5 Hz), 7.84 (*t*, 1H, *J* = 7.5 Hz), 7.98 (*t*, 1H, *J* = 8.1 Hz), 8.23–8.28 (*m*, 2H), 8.48 (*d*, 1H, *J* = 8.1 Hz), 8.69 (*d*, 1H, *J* = 7.4 Hz), 8.97 (*s*, 1H), ESI-MS *m*/*z*: 360 $[M+H]^+$. Anal. Calcd for $C_{22}H_{21}N_3O_2 \cdot 2H_2O$: C, 66.82; H, 6.37; N, 10.63. Found: C, 66.56; H, 6.53; N, 10.48.

3.1.10. 7-Oxo-7H-dibenzo[de,g]quinoline-4-carboxyl (2-(diethylamino)ethyl)amide (**5g**)

Compound **4** was treated with 2-(diethylamino)ethylamine according to general acylation procedure to give **5g** (52%) as yellow/brown solid. ^{1}H NMR ($CDCl_3$): δ_H 1.04 (*t*, 6H, *J* = 7.1 Hz), 2.62 (*q*, 4H, *J* = 7.1 Hz), 2.78 (*t*, 2H, *J* = 5.9 Hz), 3.66 (*q*, 2H, *J* = 5.5 Hz), 7.56 (*d*, 1H, *J* = 7.4 Hz), 7.74–7.83 (*m*, 2H), 8.17 (*d*, 1H, *J* = 8.0 Hz), 8.32 (*d*, 1H, *J* = 7.4 Hz), 8.43–8.48 (*m*, 2H), 9.06 (*s*, 1H); ESI-MS *m*/*z*: 374 $[M+H]^+$. Anal. Calcd for $C_{23}H_{23}N_3O_2$: C, 73.97; H, 6.21; N, 11.25. Found: C, 73.59; H, 6.37; N, 10.87.

3.1.11. 7-Oxo-7H-dibenzo[de,g]quinoline-4-carboxyl (3-(diethylamino) propyl)amide (**5h**)

Compound **4** was treated with 3-(diethylamino)propylamine according to general acylation procedure to give **5h** (64%) as yellow solid. ^{1}H NMR ($CDCl_3$): δ_H 0.90 (*t*, 6H, *J* = 7.1 Hz), 1.89 (*m*, 2H), 2.51 (*q*, 4H, *J* = 7.1 Hz), 2.69 (*t*, 2H, *J* = 5.9 Hz), 3.72(*q*, 2H, *J* = 5.5 Hz), 7.55 (*d*, 1H, *J* = 7.4 Hz), 7.73 (*d*, 1H, *J* = 7.6 Hz), 7.80 (*d*, 1H, *J* = 8.4 Hz), 8.17 (*d*, 1H, *J* = 8.0 Hz), 8.31 (*d*, 1H, *J* = 7.3 Hz), 8.43–8.49 (*m*, 2H), 9.04 (*s*, 1H), 9.16 (*m*, 1H); ESI-MS *m*/*z*: 388 $[M+H]^+$. Anal. Calcd for $C_{24}H_{25}N_3O_2 \cdot 2H_2O$: C, 68.06; H, 6.90; N, 9.92. Found: C, 67.73; H, 7.16; N, 9.67.

3.1.12. 7-Oxo-7H-dibenzo[de,g]quinoline-4-carboxyl (2-hydroxyethyl)amide (**5i**)

Compound **4** was treated with 2-hydroxy-ethylamine according to general acylation procedure to give **5i** (60%) as yellow/orange solid. ^{1}H NMR (DMSO): δ_H 3.49 (*m*, 2H), 3.64 (*m*, 2H), 2.78 (*t*, 2H, *J* = 5.9), 7.65 (*m*, 1H), 7.85–8.01 (*m*, 2H), 8.28–8.34 (*m*, 2H), 8.53–8.54 (*m*, 1H), 8.73–8.74 (*m*, 1H), 8.96–8.97 (*m*, 1H), 9.04 (s, 1H); ESI-MS *m*/*z*: 317 $[M-H]^-$. Anal. Calcd for $C_{19}H_{14}N_2O_3 \cdot H_2O$: C, 67.85; H, 4.79; N, 8.33. Found: C, 67.94; H, 4.86; N, 7.95.

3.1.13. 7-Oxo-7H-dibenzo[de,g]quinoline-4-carboxyl (3-hydroxypropyl)amide (**5j**)

Compound **4** was treated with 3-hydroxy-propylamine according to general acylation procedure to give **5j** (68%) as yellow/orange solid. ^{1}H NMR (DMSO): δ_H 1.79 (*m*, 2H), 1.89 (*m*, 2H), 3.46 (*t*, 2H, *J* = 7.0 Hz) (D_2O was added), 3.55 (*t*, 2H, *J* = 6.3 Hz), 7.62 (*t*, 1H, *J* = 7.4 Hz), 7.83 (*t*, 1H, *J* = 8.3 Hz), 7.99 (*t*, 1H, *J* = 8.3 Hz), 8.25 (*d*, 1H, *J* = 7.8 Hz), 8.30 (*d*, 1H, *J* = 8.5 Hz), 8.51 (*d*, 1H, *J* = 8.1 Hz), 8.71 (*m*, 2H, *J* = 7.4 Hz), 8.99 (*s*, 1H), 8.93 (*t*, 0.5H, *J* = 5.6 Hz); ESI-MS *m*/*z*: 333 $[M+H]^+$. Anal. Calcd for $C_{20}H_{16}N_2O_3 \cdot 2H_2O$: C, 65.21; H, 5.47; N, 7.60. Found: C, 64.87; H, 5.42; N, 7.31.

3.1.14. General procedure for the preparation of quaternary methiodide salts **6a–h**

A mixture containing 7-oxo-7*H*-dibenzo[*de*,g]quinoline-4-carboxyl (2-morpholino-ethyl)amide **5a** (0.4 g), iodomethane (1 mL), and chloroform (20 mL) is stirred at 25 °C for 24 h. The orange-yellow solid which separates is filtered, washed with chloroform, and dried in vacuo. The quaternary methiodide salt **6a** is recovered (93%) as an amorphous powder.

6a ^{1}H NMR (DMSO): δ_H 2.10–2.13 (*m*, 2H), 3.21 (*s*, 3H), 3.50 (*m*, 4H), 3.59–3.65 (*m*, 2H), 3.96 (*m*, 4H), 7.66 (*t*, 1H, *J* = 7.5 Hz), 7.88 (*t*, 1H, *J* = 7.5 Hz), 8.03 (*t*, 1H, *J* = 8.0 Hz), 8.28 (*t*, 1H, *J* = 7.6 Hz), 8.37 (*d*, 1H, *J* = 8.5 Hz), 8.57 (*d*, 1H, *J* = 8.0 Hz), 8.79 (*d*, 1H, *J* = 7.3 Hz), 9.12 (*s*, 1H), 9.07 (*t*, 1H, *J* = 5.0 Hz). ESI-MS *m*/*z*: 402 $[M]^+$.

6b ^{1}H NMR (DMSO): δ_H 2.07–2.12 (*m*, 2H), 3.20 (*s*, 3H), 3.49–3.50 (*m*, 4H), 3.58–3.63 (*m*, 4H), 3.95 (*m*, 4H), 7.68 (*t*, 1H, *J* = 7.5 Hz), 7.88 (*t*, 1H, *J* = 7.5 Hz), 8.03 (*t*, 1H, *J* = 8.0 Hz), 8.28 (*t*, 1H, *J* = 7.6 Hz), 8.37 (*d*, 1H, *J* = 8.5 Hz), 8.57 (*d*, 1H, *J* = 8.0 Hz), 8.79 (*d*, 1H, *J* = 7.3 Hz), 9.13 (*s*, 1H), 9.09 (*t*, 1H, *J* = 5.2 Hz). ESI-MS *m*/*z*: 416 $[M]^+$.

6c ^{1}H NMR (DMSO): δ_H 1.60 (*m*, 2H), 1.87 (*m*, 4H), 3.19 (*s*, 1H), 3.49 (m, 4H), 3.67 (m, 2H), 3.85–3.86 (m, 2H), 7.66 (*t*, 1H, *J* = 7.5 Hz),

7.88 (*t*, 1H, *J* = 7.5 Hz), 8.04 (*t*, 1H, *J* = 7.9 Hz), 8.28 (*t*, 1H, *J* = 7.9 Hz), 8.39 (*d*, 1H, *J* = 8.0 Hz), 8.5 8 (*d*, 1H, *J* = 8.3 Hz), 8.80 (*d*, 1H, *J* = 6.8 Hz), 9.08 (*s*, 1H), 9.25 (*m*, 1H); ESI-MS *m*/*z*: 400 $[M]^+$.

6d ^{1}H NMR (DMSO): δ_H 1.54–1.57 (*m*, 2H), 1.82 (*m*, 4H), 2.04–2.13 (*m*, 2H), 3.08 (*s*, 1H), 3.36 (*t*, 2H, *J* = 5.3 Hz) (D_2O was added), 3.48–3.52 (m, 4H), 7.62 (*t*, 1H, *J* = 7.5 Hz), 7.83 (*t*, 1H, *J* = 7.5 Hz), 7.99 (*t*, 1H, *J* = 8.0 Hz), 8.24 (*t*, 1H, *J* = 7.7 Hz), 8.34 (*d*, 1H, *J* = 8.5 Hz), 8.50 (*d*, 1H, *J* = 8.1 Hz), 8.72 (*d*, 1H, *J* = 7.5 Hz), 9.07 (*t*, 1H, *J* = 5.6 Hz), 9.09 (*s*, 1H); ESI-MS *m*/*z*: 414 $[M]^+$.

6e ^{1}H NMR (DMSO): δ_H 3.22 (*s*, 9H), 3.66 (*t*, 2H, *J* = 6.7 Hz), 3.85 (*t*, 2H, *J* = 6.3 Hz), 7.66 (*t*, 1H, *J* = 7.5 Hz), 7.88 (*t*, 1H, *J* = 7.5 Hz), 8.03 (*t*, 1H, *J* = 8.0 Hz), 8.28 (*t*, 1H, *J* = 7.6 Hz), 8.37 (*d*, 1H, *J* = 8.5 Hz), 8.57 (*d*, 1H, *J* = 8.0 Hz), 8.79 (*d*, 1H, *J* = 7.3 Hz), 9.08 (*s*, 1H). ESI-MS *m*/*z*: 360 $[M]^+$.

6f ^{1}H NMR (DMSO): δ_H 2.04–2.09 (*m*, 2H), 2.84 (*s*, 9H), 3.20 (*t*, 2H, *J* = 7.7 Hz), 3.47 (*q*, 2H, *J* = 6.4 Hz), 7.68 (*t*, 1H, *J* = 7.5 Hz), 7.90 (*t*, 1H, *J* = 7.5 Hz), 8.05 (*t*, 1H, *J* = 8.0 Hz), 8.28 (*t*, 1H, *J* = 7.6 Hz), 8.37 (*d*, 1H, *J* = 8.5 Hz), 8.57 (*d*, 1H, *J* = 8.0 Hz), 8.79 (*d*, 1H, *J* = 7.3 Hz), 9.09 (*s*, 1H), 9.08 (*t*, 1H, *J* = 5.6 Hz). ESI-MS *m*/*z*: 374 $[M]^+$.

6g ^{1}H NMR (DMSO): δ_H 1.32 (*t*, 6H, *J* = 7.2 Hz), 3.07 (*s*, 3H), 3.45 (*q*, 4H, *J* = 7.2 Hz), 3.51 (*t*, 2H, *J* = 8.0 Hz), 3.80 (*q*, 2H, *J* = 8.0 Hz), 7.68 (*t*, 1H, *J* = 7.5 Hz), 7.88 (*t*, 1H, *J* = 7.5 Hz), 8.03 (*t*, 1H, *J* = 8.0 Hz), 8.28 (*t*, 1H, *J* = 7.6 Hz), 8.37 (*d*, 1H, *J* = 8.5 Hz), 8.57 (*d*, 1H, *J* = 8.0 Hz), 8.79 (*d*, 1H, *J* = 7.3 Hz), 9.08 (*s*, 1H), 9.26 (*t*, 1H, *J* = 5.6 Hz). ESI-MS *m*/*z*: 388 $[M]^+$.

6h ^{1}H NMR (DMSO): δ_H 1.26 (*t*, 6H, *J* = 7.0 Hz), 2.00–2.05 (*m*, 2H), 2.98 (*s*, 3H), 3.32–3.36 (*m*, 6H), 3.48–3.53 (*m*, 2H), 7.68 (*t*, 1H, *J* = 7.5 Hz), 7.89 (*t*, 1H, *J* = 7.5 Hz), 8.05 (*t*, 1H, *J* = 8.0 Hz), 8.30 (*t*, 1H, *J* = 7.6 Hz), 8.37 (*d*, 1H, *J* = 8.5 Hz), 8.57 (*d*, 1H, *J* = 8.0 Hz), 8.79 (*d*, 1H, *J* = 7.3 Hz), 9.08–9.11 (*m*, 2H). ESI-MS *m*/*z*: 402 $[M]^+$.

3.1.15. 9-(3-Piperidinopropionamido)-1-azabenzanthrone (**11**)

To a stirred refluxing suspension of 9-(3-chloropropionamido)-1-azabenzanthrone (0.5 g, 1.5 mmol) and NaI (0.15 g) in EtOH (40 mL) was added dropwise piperidine (1.0 mL) in EtOH (10 mL). The mixture was stirred at reflux for 3 h, cooled to 0 °C, filtered, and washed with ether and water. The crude solid was purified by column chromatography with chloroform/methanol (100:3) elution to afford a yellow solid compound **11** (75%). ^{1}H NMR ($CDCl_3$): δ_H 1.75 (*m*, 2H), 1.80 (*m*, 4H), 2.56–2.60 (*m*, 6H), 2.73 (*t*, 2H, *J* = 6.2 Hz), 7.68 (*d*, 1H, *J* = 5.6 Hz), 7.87 (*t*, 1H, *J* = 7.3 Hz), 8.12 (*d*, 1H, *J* = 8.2 Hz), 8.18 (*d*, 1H, *J* = 2.3 Hz), 8.35 (*dd*, 1H, J_1 = 8.7 Hz and J_2 = 2.3 Hz), 8.62 (*d*, 1H, *J* = 7 .2 Hz), 8.72 (*d*, 1H, *J* = 5.6 Hz), 8.83 (*d*, 1H, *J* = 8.7 Hz), 11.82 (*s*, 1H, –CONH); ESI-MS *m*/*z*: 386 $[M + H]^+$. Anal. Calcd for $C_{24}H_{23}N_3O_2 \cdot H_2O$: C, 71.44; H, 6.25; N, 10.41. Found: C, 71.33; H, 6.32; N, 10.48.

3.1.16. Quaternary methiodide salts (**7a**)

A mixture containing compound **11** (0.5 g), iodomethane (1 mL), and chloroform (20 mL) is stirred at 25 °C for 24 h. The orange-yellow solid which separates is filtered, washed with chloroform, and dried in vacuo. The quaternary methiodide salt **7a** is recovered (88%) as an amorphous powder. ^{1}H NMR (DMSO): δ_H 1.55–1.62 (*m*, 2H), 1.82–1.87 (*m*, 4H), 3.00 (*t*, 2H, *J* = 7.5 Hz), 3.07 (*s*, 3H), 3.40 (*t*, 4H, *J* = 4.8 Hz), 3.75 (*t*, 2H, *J* = 7.8 Hz), 8.01 (*d*, 1H, *J* = 5.7 Hz), 8.03–8.08 (*m*, 2H), 8.44 (*d*, 1H, *J* = 8.1 Hz), 8.54–8.57 (*m*, 2H), 8.76–8.79 (*m*, 2H), 10.69 (*s*, 1H, –CONH); ESI-MS *m*/*z*: 400 $[M]^+$. Anal. Calcd for $C_{25}H_{26}N_2O_2N^+I^-$: C, 56.93; H, 4.97; N, 7.97. Found: C, 56.72; H, 4.99; N, 8.22.

3.1.17. 7-Oxo-7H-dibenzo[de,g]quinoline (**8**)

^{1}H NMR (DMSO): δ_H 7.65 (t, 1H, *J* = 8.0 Hz), 7.86 (t, 1H, *J* = 8.0 Hz), 7.96 (t, 1H, *J* = 7.6 Hz), 8.19 (*d*, 1H, *J* = 8.0 Hz), 8.27 (*d*, 1H, *J* = 5.3 Hz), 8.30 (*d*, 1H, *J* = 7.6 Hz), 8.54 (*d*, 1H, *J* = 8.0 Hz), 8.72 (*d*, 1H, *J* = 7.0 Hz), 9.00 (*d*, 1H, *J* = 5.3 Hz); ESI-MS *m*/*z*: 232 $[M + H]^+$. Anal. Calcd for $C_{16}H_9NO$: C, 83.10; H, 3.92; N, 6.06. Found: C, 82.87; H, 3.65; N, 5.89.

3.2. Biological activity and molecular modeling

3.2.1. In vitro *inhibition studies on AChE and BuChE*

All the assays were under 0.1 M KH_2PO_4/K_2HPO_4 buffer, pH 8.0, using a Shimadzu 2450 Spectrophotometer. Enzyme solutions were prepared to give 2.0 units/mL in 2 mL aliquots. The assay medium contained phosphate buffer, pH 8.0 (1 mL), 50 μL of 0.01 M DTNB, 10 μL of enzyme, and 50 μL of 0.01 M substrate (acetylthiocholine chloride). The substrate was added to the assay medium containing enzyme, buffer, and DTNB with inhibitor after 15 min of incubation time. The activity was determined by measuring the increase in absorbance at 412 nm for 1 min interval at 37 °C. Calculations were performed according to the method of the equation in Ellman et al. [22].

In vitro BuChE assay uses the similar method described above.

3.2.2. Molecular modeling

The initial model of AChE for docking studies was built based on the X-ray crystal structure of the bis(5)tacrine–AChE complex which was obtained from the Protein Data Bank (PDB entry 2CMF). The original ligand was removed while water molecules present in the PDB file were maintained in their position. 3D structures of the oxoisoaporphine derivatives were generated and optimized by Discovery Studio 1.7 package (Accelrys Inc., San Diego, CA). AutoDock 3.0.5 [33] package was used to perform docking simulations, which adopts the hybrid Lamarckian Genetic Algorithm as searching algorithm and allows full flexibility of the ligand. Solvation parameters and Kollman charges for all atoms in AChE were assigned by using AutoDock Tools. The grid for energy evaluation was centered at residue Trp 84 in AChE with grid points in the *x*-, *y*-, *z*-axes set to 50 × 50 × 50 and separated by 0.375 Å. The initial population size and maximum number of energy evaluations were set to 100 and 1.0 × 107 respectively. The docked results within an RMSD of 1.5 Å were clustered, and the final results of each ligand were selected considering both the embedded empirical binding free energy evaluation and the clustering analysis.

The results from docking studies were used as the starting model of molecular dynamics (MD) simulations. After importing the complex structure into Discovery Studio 1.7 package, necessary modifications were carried out including correcting the protonation states of the residues and converting the water molecules into TIP3P model. A 20 × 20 × 20 Å explicit TIP3P water box which centered at residue Phe 330 was then created in each complex model, immersing the whole active site. The CHARMm [34] force field parameter was assigned to each atom and the whole system was then submitted to two rounds of 2000 steps of energy minimization (steepest descent and conjugate gradient). Harmonic restraints were applied to the atoms 8 Å from the active gorge while coordinates of atoms 12 Å away from the active gorge were fixed during the subsequent study. The system then underwent 20 ps of NVT MD simulations, heating the entire system from 0 to 300 K. After 50 ps of equilibration phase, 0.5 ns of production simulation were carried out in 300 K. SHAKE algorithm was applied to freeze all hydrogen bonds, and time step of the simulation was set to 2 fs. The MD average structure of the last 100 ps was energy minimized by 2500 steps of conjugate gradient minimization to an rms of the gradient of 0.001 kcal/mol/Å.

Acknowledgements

We thank the Natural Science Foundation of China (20772159), the NSFC/RGC Joint Research Scheme (Grants 30731160006), the

Science Foundation of Guangzhou (2006Z2-E402), the Science Foundation of Zhuhai (Grant PC20041131), and the NCET for financial support of this study.

References

[1] R. Cacabelos, A. Alvarez, V. Lombardi, L. Fernández-Novoa, L. Corzo, P. Pérez, et al., Drugs Today 36 (2000) 415–499.
[2] P.T. Francis, A.M. Palmer, M. Snape, G.K. Wilcock, J. Neurol. Neurosurg. Psychiatr. 66 (1999) 137–147.
[3] A. Castro, A. Martinez, Mini-Rev. Med. Chem. 1 (2001) 267–272.
[4] P. Taylor, Neurology 51 (1998) S30–S35.
[5] C. Viegas Jr., V.da S. Bolzani, E.J. Barreiro, C.A.M. Fraga, Mini-Rev. Med. Chem. 5 (2005) 915–926.
[6] J. Hardy, D.J. Selkoe, Science 297 (2002) 353–356.
[7] G.V. De Ferrari, M.A. Canales, I. Shin, L.M. Weiner, I. Silman, N.C. Inestrosa, Biochemistry 40 (2001) 10447–10457.
[8] M.L. Bolognesi, V. Andrisano, M. Bartolini, A. Cavalli, A. Minarini, M. Recanatini, et al., Il Farmaco 60 (2005) 465–473.
[9] M.I. Rodriguez-Franco, M.I. Fernandez-Bachiller, C. Perez, B. Hernandez-Ledesma, B. Bartolome, J. Med. Chem. 49 (2006) 459–462.
[10] E.H. Rydberg, B. Brumshtein, H.M. Greenblatt, D.M. Wong, D. Shaya, L.D. Williams, et al., J. Med. Chem. 49 (2006) 5491–5500.
[11] N. Akula, L. Lecanu, J. Greeson, V. Papadopoulos, Bioorg. Med. Chem. Lett. 16 (2006) 6277–6280.
[12] H. Tang, F.-X. Ning, Y.-B. Wei, S.-L. Huang, Z.-S. Huang, A.S.-C. Chan, et al., Bioorg. Med. Chem. Lett. 17 (2007) 3765–3768.
[13] H. Guinaudeau, J. Nat. Prod. 57 (1994) 1033–1135.
[14] X. Dong, I.O. Mondranondra, C.T. Che, H.H.S. Fong, N.R. Farnsworth, Pharm. Res. 6 (1989) 637–640.
[15] D. Warthen, E.L. Gooden, M. Jacobson, J. Pharm. Sci. 58 (1969) 637–638.
[16] A.M. Clark, E.S. Watson, M.K. Ashfaq, C.D. Hufford, Pharm. Res. 4 (1987) 495–498.
[17] C.D. Hufford, M.J. Funderburk, J.M. Morgan, L.W. Robertson, J. Pharm. Sci. 64 (1975) 789–792.
[18] D.N. Nicolaides, G.K. Papageorgiou, J. Stephanidou-Stephanatou, Tetrahedron 45 (1989) 4585–4592.
[19] B. Neises, W. Steglich, Angew. Chem. 90 (1978) 556–557.
[20] C. Guillonneau, A. Pierre, Y. Charton, N. Guilbaud, L. Kraus-Berthier, S. Leonce, et al., J. Med. Chem. 42 (1999) 2191–2203.
[21] J. Martinez, J.P. Bali, M. Rodriguez, B. Castro, R. Magous, J. Laur, et al., J. Med. Chem. 18 (1985) 1874–1879.
[22] G.L. Ellman, K.D. Courtney, V. Andres Jr., R.M. Featherstone, Biochem. Pharmacol. 7 (1961) 88–92.
[23] M. Harel, I. Schalk, L. Ehret-Sabatier, F. Bouet, M. Goeldner, C. Hirth, et al., Proc. Natl. Acad. Sci. U.S.A. 90 (1993) 9031–9035 PDB ID: 1ACL.
[24] J. Massoulie, J. Sussman, S. Bon, I. Silman, Prog. Brain Res. 98 (1993) 139–146.
[25] A. Fersht, Enzyme Structure and Mechanism, W.H. Freeman Company, Reading, England/San Francisco, 1977.
[26] N.C. Inestrosa, A. Alvarez, C.A. Perez, R.D. Moreno, M. Vicente, C. Linker, et al., Neuron 16 (1996) 881–891.
[27] M. Bartolini, C. Bertucci, V. Cavrini, V. Andrisano, Biochem. Pharmacol. 65 (2003) 407–416.
[28] Y. Nicolet, O. Lockridge, P. Masson, J.C. Fontecilla-Camps, F. Nachon, J. Biol. Chem. 278 (2003) 41141–41147.
[29] J. Munoz-Muriedas, J.M. Lopez, M. Orozco, F.J. Luque, Curr. Pharm. Des. 10 (2004) 3131–3140.
[30] W.L. DeLano, The PyMOL Molecular Graphics System, DeLano Scientific: San Carlos, CA.
[31] A. Krammer, P.D. Kirchhoff, X. Jiang, C.M. Venkatachalam, M. Waldman, J. Mol. Graph. Model 23 (2005) 395–407.
[32] D.K. Gehlhaar, G.M. Verkhivker, P.A. Rejto, C.J. Sherman, D.B. Fogel, L.J. Fogel, et al., Chem. Biol. 2 (1995) 317–324.
[33] D.S. Goodsell, A.J. Olson, Proteins 8 (1990) 195–202.
[34] B.R. Brooks, R.E. Bruccoleri, B.D. Olafson, D.J. States, S. Swaminathan, M. Karplus, J. Comput. Chem. 4 (1983) 187–217.